A Tale of Tails: Alkyl Chain Directed Formation of 2D Porous Networks Reveals Odd–Even Effects and Unexpected Bicomponent Phase Behavior

Elke Ghijsens,[†,‡] Oleksandr Ivasenko,[†,‡] Kazukuni Tahara,[§] Hiroyuki Yamaga,[§] Shintaro Itano,[§] Tatyana Balandina,[‡] Yoshito Tobe,[§,*] and Steven De Feyter[‡,*]

[‡]Department of Chemistry, Division of Molecular Imaging and Photonics, KU Leuven, Celestijnenlaan 200 F, B-3001 Leuven, Belgium and [§]Division of Frontier Materials Science, Graduate School of Engineering Science, Osaka University, Toyonaka, Osaka 560-8531, Japan. [†]These authors contributed equally.

ABSTRACT Supramolecular self-assembly of suitably functionalized building blocks on surfaces can serve as an excellent test-bed to gain understanding and control over multicomponent self-assembly in more complex matter. Here we employ a powerful combination of scanning tunnelling microscopy (STM) and molecular modeling to uncover two-dimensional (2D) crystallization and mixing behavior of a series of alkylated building blocks based on dehydrobenzo[12]annulene, forming arrays of nanowells. Thorough STM investigation employing high-resolution spatial imaging, use of specially designed marker molecules, statistical analysis and thermal stability measurements revealed rich and complex supramolecular chemistry, highlighting the impact of odd–even effects on the phase behavior. The methodology and analysis presented in this work can be easily adapted to the self-assembly of other alkylated building blocks.

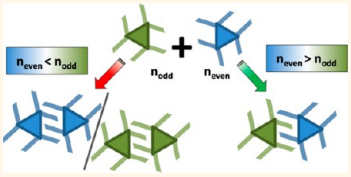

KEYWORDS: chirality · odd–even · self-assembly · multicomponent

Many applications involve the interaction of molecules with surfaces. Patterning surfaces in view of tuning its interfacial properties can be realized *via* the templating with organic molecules.[1−7] Bestowing self-assembled monolayers (SAMs) to the surface is an inexpensive and versatile bottom-up method.[8−13] Understanding and controlling the phase behavior on adsorption onto a solid support is important in developing robust strategies for engineering interfaces. In general, the coadsorption of the components present in the liquid mixture can lead to several possibilities.[14−18] The compounds can display eutectic behavior.[19,20] As such, the molecules are adsorbed in separate phases, each representing a structure identical to the pure system. When one of the compounds, however, gets incorporated in the lattice of the other one, mixing on the surface occurs. Depending on whether this mixing happens in an ordered or random fashion, cocrystallization or ideal mixing behavior, respectively, is seen on the surface.[21,22] Predicting the assembling behavior of multicomponent mixtures on solid surfaces is particularly challenging.[23]

Very subtle structural differences in the binary mixing partners may yield surprising results.[24,25] For instance, binary mixtures of primary linear alcohols that differ by a single methylene group unveil ideal mixing if the shorter alcohol possesses an odd amount of carbon atoms.[26,27] In contrast, if the shorter component is "even", cocrystals are formed.[26,27] The fact that both components mix (random or ordered) on the surface finds its origin in the similar symmetries of the unit cells of the pure components.[23]

In contrast, linear alkanes that differ only 1 carbon atom will mainly phase separate due to the difference in the crystal structure of odd (*pgg* space group) and even (*cm* arrangement) compounds.[28,29] The difference in space group mainly finds origin in a different orientation of the terminal groups of the alkanes and is driven by minimizing the intermolecular steric repulsion. In general, many high-density organic thin films show an alteration of the network properties and structure depending on the

* Address correspondence to tobe@chem.es.osaka-u.ac.jp; steven.defeyter@chem.kuleuven.be.

Received for review June 24, 2013 and accepted August 21, 2013.

Published online August 21, 2013
10.1021/nn4032036

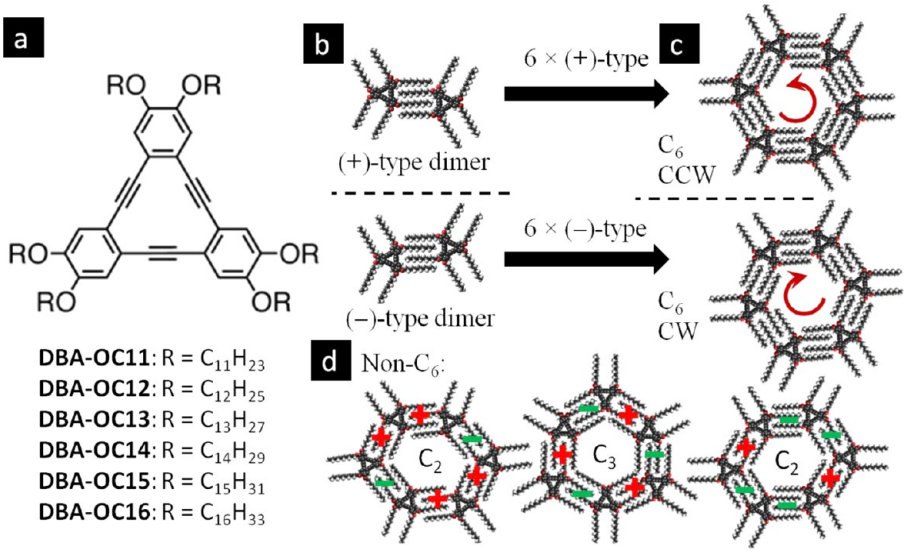

Figure 1. (a) Chemical structures of the achiral DBA compounds tested in this study. Expression of supramolecular chirality at the level of interdigitated DBA dimers (b), C_6-symmetric hexamers (c), and selected DBA hexamers with lower symmetry (d). The C_6-CW and CCW pore can also be distinguished by the orientation of the alkyl chains at the rim of pore. The (+) and (−) signs in (d) indicate the chirality of each interdigitation pattern.

parity of the number of the CH_2-units in the alkyl chains, a result called the *odd−even effect*.[30−34] Odd−even effects may also have an impact on the chiral nature of such monolayer-thin films.[35−38]

The question rises if the subtle phenomena obtained for simple systems are general and also hold for more complex systems. Popular and important two-dimensional (2D) networks are those containing void spaces arranged regularly in the nanometer range, the so-called low-density 2D porous networks.[2,39−42]

Recently we showed the possibility of achiral triangular dehydrobenzo[12]annulene (DBA) derivatives to use as a model system to study various aspects of molecular self-assembly on surfaces.[43] Mixing of achiral DBA derivatives with an even number of carbon atoms per alkoxy chain, but that differ in the length of the alkoxy chains, leads to nearly complete mixing when the difference in alkoxy chain length is two and to phase separation when the difference in alkoxy chain length reaches four methylene groups.[44]

In this article, we investigate the phase behavior of equimolar binary mixtures of alkoxylated triangular dehydrobenzo[12]annulene (DBA) derivatives that differ only in 1 carbon atom in length.

The factors that are at the origin of their peculiar phase behavior are unraveled, and also the structural properties of the monocomponent systems are investigated in detail, revealing intriguing odd−even effects that also have an impact on monolayer chirality. The study is performed at the liquid−solid interface and examines the structural aspects of the porous networks upon physisorption of the DBA compounds from the solution phase. The networks are probed by scanning tunneling microscopy (STM) and modeled *via* density functional theory (DFT) and molecular mechanics (MM) simulations.

RESULTS

Description of the Model Systems and Basic Terminology. For this study we have chosen homologous derivatives of dehydrobenzo[12]annulenes (**DBA-OCn**) with alkoxy chains varied from undecyloxy (**DBA-OC11**) to hexadecyloxy (**DBA-OC16**, Figure 1a). Syntheses of **DBA-OC11** and **DBA-OC15** were reported here (Supporting Information, section S11). Synthesis of the other compounds were reported previously.[45,46] The solutions were prepared by mixing **DBA-OCn$_{odd}$** (**DBA-OC11**, **DBA-OC13**, or **DBA-OC15**) with **DBA-OCn$_{even}$** (**DBA-OC12**, **DBA-OC14**, or **DBA-OC16**) in a 1:1 molar ratio, dissolved in 1-phenyloctane. As such, five bicomponent mixtures of DBAs that differ by only one carbon atom in length were probed: **DBA-OC11/DBA-OC12** (2.5×10^{-6} M), **DBA-OC12/DBA-OC13** (2.5×10^{-6} M), **DBA-OC13/DBA-OC14** (8.3×10^{-7} M), **DBA-OC14/DBA-OC15** (8.3×10^{-7} M), and **DBA-OC15/DBA-OC16** (8.3×10^{-7} M). The total concentrations are described in the parentheses.

The structure of the honeycomb-pores is a consequence of two possible mirror-image interdigitation patterns stabilizing the supramolecular network. At the level of the DBA (homo or hetero) dimers, the (−)-type interdigitation can be easily distinguished from its enantiomer, the (+)-type interdigitation pattern (Figure 1b). Hexagonal pores built exclusively from (−) or (+) interdigitation have C_6-symmetry and are denoted as CW (*i.e.*, "clock-wise") or CCW (*i.e.*, "counterclockwise"), respectively. Non-C_6 hexagonal pores can also be formed by combination of (+) and (−) interdigitation patterns: out of the 12 possible such

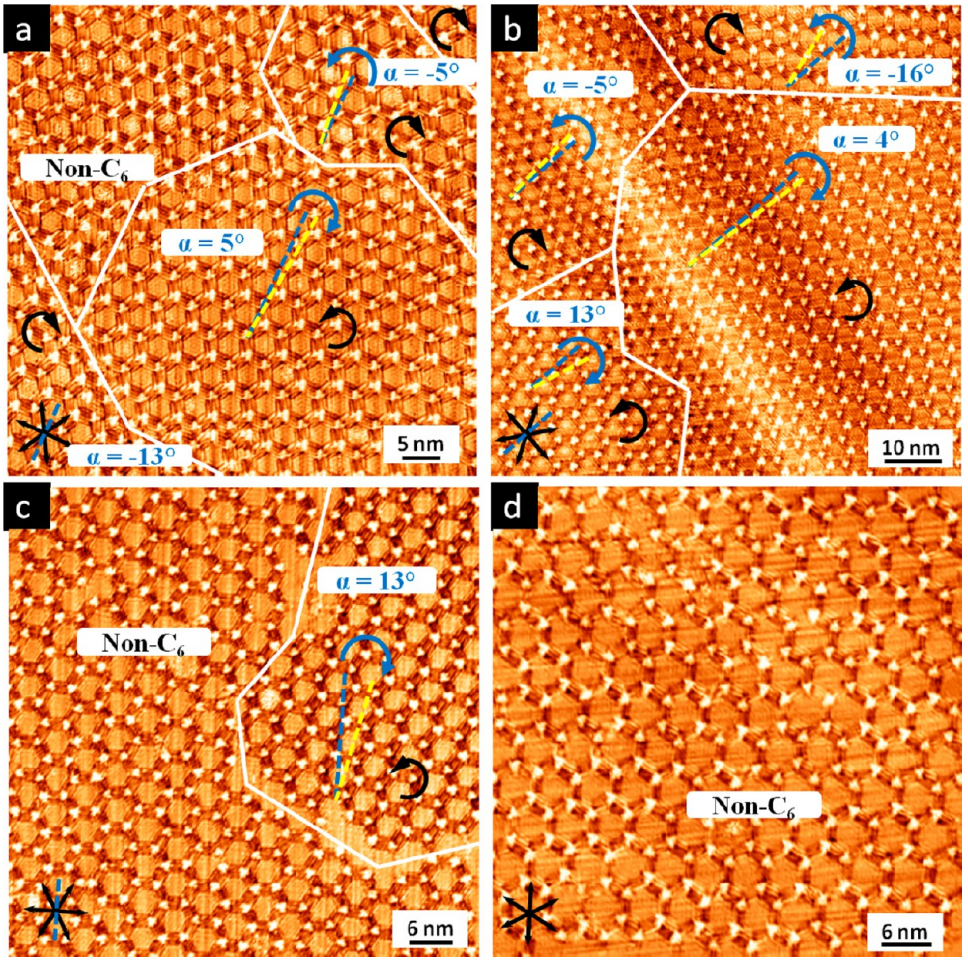

Figure 2. Typical STM images of binary 1:1 mixtures of DBA-OCn$_{odd}$ and DBA-OCn$_{even}$. (a, b) STM images of DBA-OC12/DBA-OC13 (I_{set} = 0.2 nA and V_{bias} = −0.2 V for both images). The surface is mainly covered with domains of CW or CCW hexagons. The angle α represents the angle between the unit cell vector (yellow dashed line) and the ⟨1$\bar{1}$00⟩ directions of HOPG (blue dashed line). (c, d) STM images of DBA-OC15/DBA-OC16. The surface is mainly covered with non-C_6-symmetric hexagons. The domain borders are highlighted by the white lines. The black arrows in the left corner represent the main symmetry directions of HOPG.

combinations C_2- and C_3-symmetric are the most common (Supporting Information, Figure S10).

Self-Assembly of Binary Mixtures Containing Both DBA-OCn$_{odd}$ and DBA-OCn$_{even}$. STM images (Figure 2 and Supporting Information, section S2) show that upon adsorption porous networks are formed for all mixtures. Surprisingly though, detailed analysis (Supporting Information, section S3) of the relative abundance of different types of hexagonal pores suggests that the behavior on the surface could be split in two groups (Figure 3). When the **DBA-OCn$_{even}$** compound is smaller than the **DBA-OCn$_{odd}$** (*i.e.*, **DBA-OC12/DBA-OC13** and **DBA-OC14/DBA-OC15** mixtures), the surface is mainly covered with domains consisting of C_6-hexagons (Figure 2a,b; Supporting Information, Figure S3). In contrast, when the binary mixture consists of a **DBA-OCn$_{odd}$** compound that is smaller than the **DBA-OCn$_{even}$** (*i.e.*, **DBA-OC11/DBA-OC12**, **DBA-OC13/DBA-OC14**, and **DBA-OC15/DBA-OC16** solutions), the surface is mainly covered with DBA hexagons of lower symmetry (Figure 2c,d and Figures S1 and S2).

While this analysis is a clear signature of differences between the respective mixtures, the exact adlayer composition cannot be concluded. In general, self-assembly from a multicomponent solution can lead to preferential adsorption, phase separation, cocrystallization or random mixing of different components on the surface. Unfortunately, direct assignment of the identity of adsorbed DBAs is not straightforward because in each mixture two components differ only by a single methylene group. To understand the peculiar self-assembly behavior of the binary mixtures, we investigated in detail the corresponding monocomponent assemblies at the 1-phenyloctane/HOPG interface.

Self-Assembly of Monocomponent DBA Systems. All studied DBAs form porous networks (Figure 4) with significant abundance of C_6-symmetric pores (Table 1 and section S4).

The precision of STM measurements is enough to distinguish differences in unit cell parameters of the DBA assemblies; however, it is much more convenient and reliable to use the unit cell alignment angle α with respect to the HOPG lattice. Indeed, the angle α of CW/CCW domains is structure specific and varies greatly between DBAs of different parity (Table 1), yielding mean average of 13° for **DBA-OCn$_{odd}$** and 4.5° for **DBA-OCn$_{even}$**.

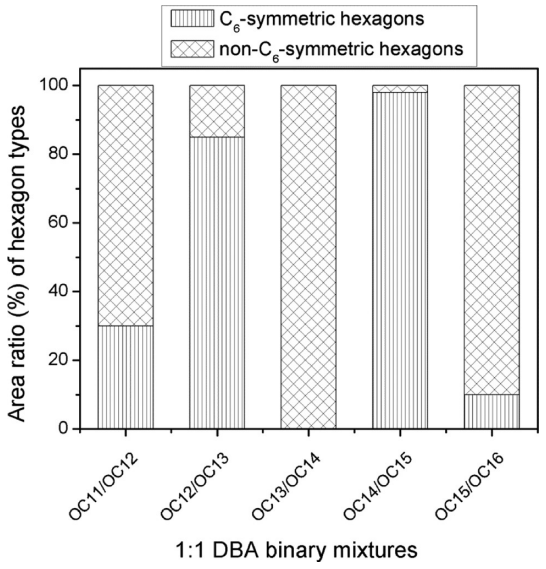

Figure 3. Ratio between the surface coverage of the C_6- and the non-C_6-symmetric hexagonal pores for equimolar mixtures of different DBAs. The behavior on the surface can be split in two groups depending on whether the DBA-OCn$_{odd}$ or DBA-OCn$_{even}$ is larger.

Mixing and Phase Separation in Bicomponent DBA Assemblies. Analysis of the alignment angle α in the ordered assemblies formed from **DBA-OC12**/**DBA-OC13** and **DBA-OC14**/**DBA-OC15** mixtures show clear bimodal distribution with maxima corresponding to the alignment angle of pure components (Figure 5 and Table 1). Thus, self-assembly from DBA mixtures in which **DBA-OCn$_{odd}$** is larger than **DBA-OCn$_{even}$** leads to phase separation on the surface. Interestingly, there appears to be a preference in the adsorption of the smaller **DBA-OCn$_{even}$**.

Unfortunately, similar analysis cannot be directly applied to DBA mixtures in which **DBA-OCn$_{odd}$** is smaller than **DBA-OCn$_{even}$** because of disorder present in those assemblies. However, the disorder is in itself an evidence of random mixing of both components on the surface since monocomponent systems tend to form highly ordered hexagonal networks.

To gain structural insights into phase behavior of bicomponent DBA assemblies at the molecular level

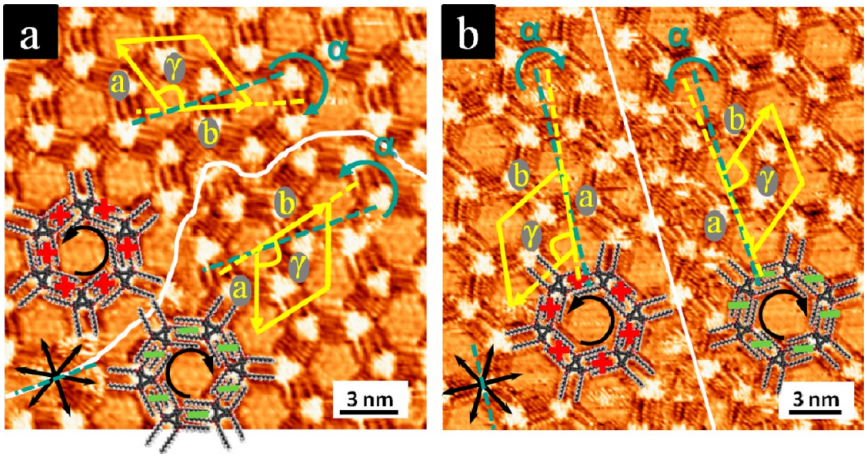

Figure 4. High resolution STM-images of mirror image domains of (a) DBA-OC11 (I_{set} = 0.2 nA and V_{bias} = −0.2 V) and (b) DBA-OC12 (I_{set} = 0.2 nA and V_{bias} = −0.2 V). Unit cells are indicated in yellow. The HOPG main symmetry directions are represented by the black arrows in the left corner. The HOPG reference axis used to measure the angle α is highlighted in blue. In this assignment CW and CCW domains have +α and −α, respectively, with the absolute value of α being characteristic to the given DBA-OCn.

TABLE 1. Measured Characteristics of the Structure of Mono-Component DBA Assemblies

	unit cell parameters			alignment angle	ratio of hexagons		
compound	*a* (nm)	*b* (nm)	γ (deg)	α (deg)	C_6-CCW (%)	non-C_6 (%)	C_6-CW (%)
DBA-OC11	4.3 ± 0.1	4.2 ± 0.1	120 ± 1	13.9 ± 1.4	47 ± 3	0.3 ± 0.1	52 ± 3
DBA-OC12	4.5 ± 0.1	4.6 ± 0.1	120 ± 1	4.7 ± 1.3	54 ± 4	0.4 ± 0.3	46 ± 4
DBA-OC13	4.8 ± 0.1	4.7 ± 0.1	120 ± 1	13.2 ± 1.3	32 ± 13	28 ± 9	40 ± 4
DBA-OC14	5.0 ± 0.1	5.0 ± 0.1	120 ± 1	4.5 ± 1.3	50 ± 1	0.9 ± 0.8	49 ± 1
DBA-OC15	5.2 ± 0.2	5.2 ± 0.1	120 ± 1	12.2 ± 0.5	46 ± 3	4.9 ± 2.0	49 ± 4
DBA-OC16	5.5 ± 0.1	5.4 ± 0.2	121 ± 1	4.3 ± 0.6	55 ± 11	2.1 ± 1.2	43 ± 11

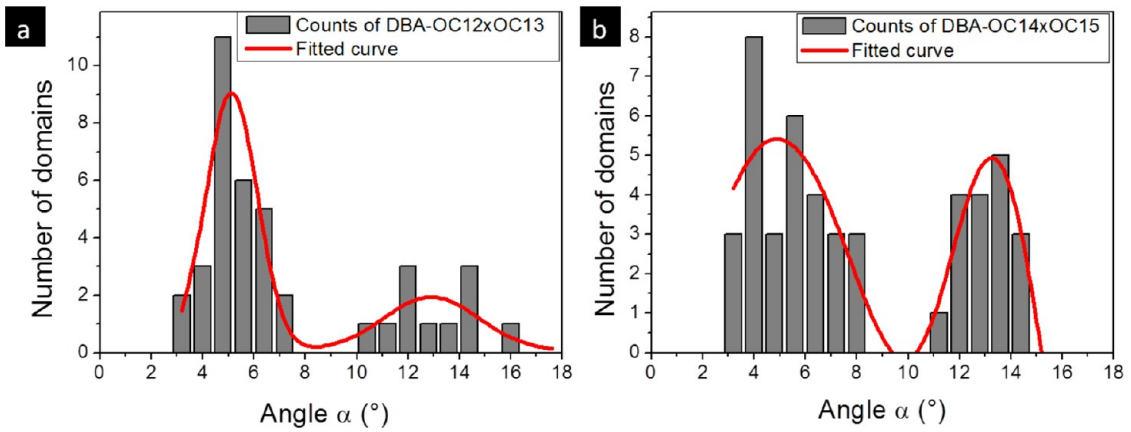

Figure 5. Bimodal fitted distribution of the absolute angle α (angle between the unit cell vector and the normals of HOPG) for chiral (CW and CCW) domains in binary DBA samples with DBA-OCn$_{even}$ < DBA-OCn$_{odd}$. (a) The equimolar mixture DBA-OC12/DBA-OC13 shows peak maxima at 5.1 and 12.9°. (b) The equimolar mixture DBA-OC14/DBA-OC15 has the peak maxima located at 4.9 and 13.5°.

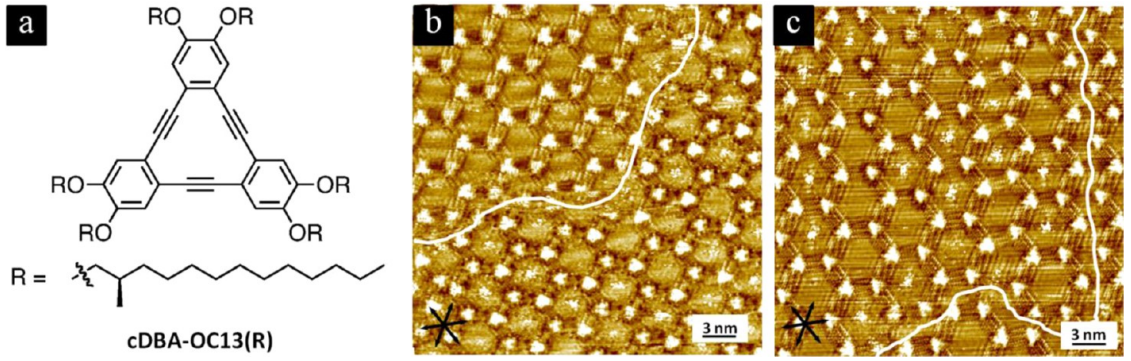

Figure 6. (a) Chemical structure of chiral cDBA-OC13(R). This molecule can be recognized in STM images by a black contour surrounding the bright triangular core of the DBA molecule. (b) STM-image of the monolayer adsorbed from the solution mixture of DBA-OC12 and cDBA-OC13(R), a chiral DBA with a stereocenter in each alkoxy group (I_{set} = 0.17 nA and V_{bias} = −0.23 V). The upper domain contains molecules without any black contours. In contrast, the lower domain contains mainly molecules surrounded by a black contour. The mixture has a tendency to phase separate. (c) STM-image of the monolayer adsorbed from the solution mixture cDBA-OC13(R)/DBA-OC14 (I_{set} = 0.18 nA and V_{bias} = −0.32 V). Black contour molecules are clearly adsorbed in a domain of DBA-OC14. On the surface both molecules rather mix. The white line represents a domain border. The black arrows represent the graphite main symmetry directions.

we have studied the self-assembly of **DBA-OC12** and **DBA-OC14** with **cDBA-OC13(R)**, a DBA with a stereocenter in each alkoxy chain. The latter one is readily distinguishable in STM images as it appears with a black contour (Figure 6).[46] Potential origins of this peculiar contrast are the conformation of the functional groups as well as its relative position with respect to the graphite surface.

Surface distribution of **cDBA-OC13(R)** directly confirms phase separation and random mixing in the case of **cDBA-OC13(R)/DBA-OC12** and **cDBA-OC13(R)/DBA-OC14**, respectively. Furthermore, while small amounts of shorter **DBA-OC12** can be observed in the phase of **cDBA-OC13(R)**, the opposite-inclusion of **cDBA-OC13(R)** into **DBA-OC12** does not happen.

Thermal Annealing of the Mono- and Bicomponent DBA Assemblies. In self-assembly on surfaces, the observed structures do not always represent thermodynamic equilibrium. To differentiate thermodynamically stable assemblies from those that are metastable (kinetically trapped), we have performed a series of experiments at higher temperatures.

Thermal annealing of monocomponent systems leads to disappearance of the lower symmetry (C_1-, C_2-, C_3-) hexagons, yielding larger domains of the perfectly ordered hexagonal networks of the DBAs (Supporting Information, section S7). Similar effects were observed in self-assembly at elevated temperatures of DBA mixtures in which **DBA-OCn$_{odd}$** was larger than **DBA-OCn$_{even}$**. Specifically, at higher temperatures, all non-C_6-symmetric pores, which coexisted when the monolayers were prepared at room temperature, disappeared, leaving on the surface only large separated phases of pure components. Interestingly, even so, self-assembly was always done from equimolar mixtures; at elevated temperatures there was significant preferential adsorption (>90%) of shorter DBAs (Supporting Information, section S8).

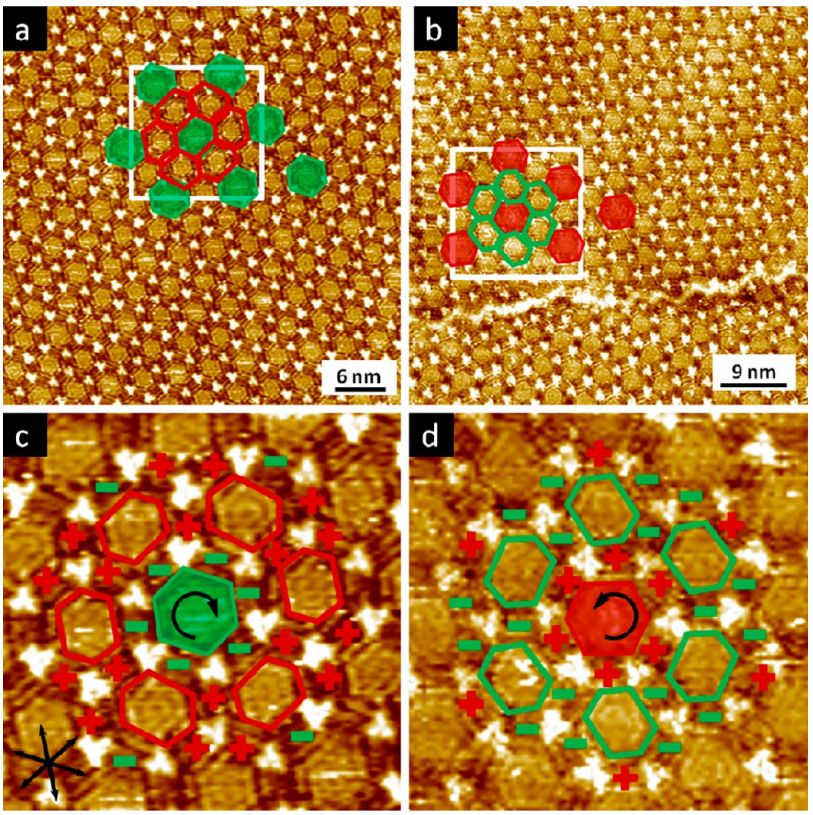

Figure 7. STM images (I_{set} = 0.2 nA and V_{bias} = −0.2 V) of the 1:1 binary mixture of DBA-OC11/DBA-OC12 after thermal annealing at 80 °C. (a, b) New chiral superstructure is observed containing ordered combination of chiral C_6- (solid green or red) and achiral C_2-symmetric (open green or red) hexagons. Both mirror-handed superlattices are seen on the surface. (c, d) The images below are the enlarged areas inside the white squares of the top images. The graphite main symmetry directions are represented by the black arrows in the left corner. All alkyl chains lie parallel to the HOPG main symmetry directions.

TABLE 2. Short Summary of Self-Assembly of Binary Mixtures of DBAs

$n_{odd} > n_{even}$		$n_{odd} < n_{even}$	
RT	**annealed at 80 °C**	**RT**	**annealed at 80 °C**
phase separation, non-C_6-symmetric pores are randomly distributed	phase separation, preferential adsorption of **DBA-OCn$_{even}$**, non-C_6-symmetric pores are absent	random mixing, non-C_6-symmetric pores are majority	ordered coassembly, of C_6-symmetric pores of **DBA-OCn$_{even}$** and C_2-symmetric mixed pores

The most unexpectedly, thermal annealing of mixed self-assemblies in which **DBA-OCn$_{even}$** was larger than **DBA-OCn$_{odd}$** led to the formation of a new highly ordered structure comprising both C_6- and C_2-symmetric pores (Figure 7). This structure has two distinct sites: (A) DBAs forming C_6-symmetric rings and (B) single DBAs joining such rings into the perfectly hexagonal superstructure. Such superstructure was never observed in the self-assembly of single component systems and thus has to contain both components. Finally, experiments with marker molecules (**cDBA-OC13(R)**/**DBA-OC14** mixtures) have allowed to identify that in the superstructure **DBA-OCn$_{even}$** and **DBA-OCn$_{odd}$** occupy A and B sites, respectively (Supporting Information, section S8). All these results are summarized in Table 2.

DISCUSSION

The complex behavior in DBA assemblies presented above does not fit into any single known model and requires detailed insight into self-assembly structure at the molecular level. For this we performed a series of molecular modeling calculations.

Optimization of isolated DBA molecules *in vacuo* showed D_{3h}-symmetric structure with flat aromatic core and nonparallel diverging alkyl chains in all-*trans* conformation (Figure 8a).

Upon adsorption of DBA its molecular symmetry changes to C_3. Now the alkyl chains run parallel in pairwise fashion and are coaligned with the main symmetry directions of HOPG. Optimization of the substrate−molecule interactions matches the placement

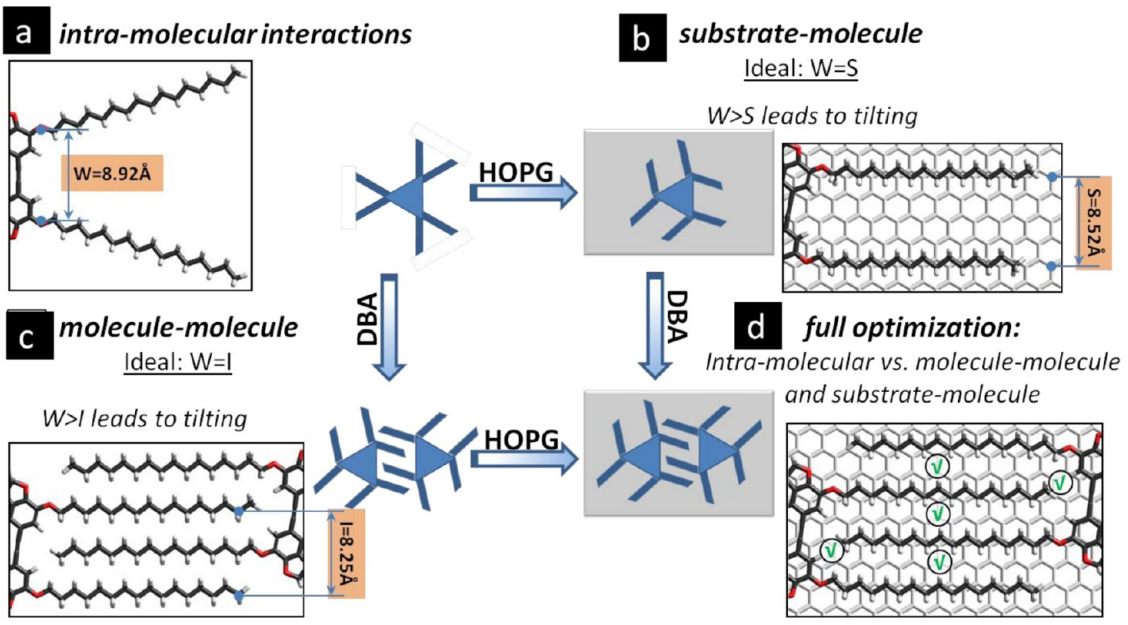

Figure 8. Relationship between various types of supramolecular interactions present in DBA self-assembly: (a) geometry of single DBA, fully relaxed *in vacuo*, showing nonparallel alkyl chains diverging away from the core (*W* is the "width" of DBA core- distance between the alkyl chains when they are orthogonal to the side of DBA triangle); (b) effect of surface- adsorption of single DBA on HOPG surface (*S* is the distance between the equivalent sites of HOPG surface); (c) structure of DBA dimers *in vacuo* as the result of interplay between optimization of intermolecular interactions and building up intramolecular strain (*I* is the distance between DBA alkyl chains in perfectly interdigitating DBA dimer) and (d) fully optimized geometry of DBA dimers on HOPG as the result of interplay between intra-, inter-, and substrate−molecule interactions. Both molecule−molecule (marked with green ticks: matching interdigitation between all alkyl chains and optimal distance between the methyl groups and the DBA cores) and substrate−molecule interactions are responsible for generation of molecular chirality (tilt of alkyl chains with respect to building block core) of DBA assemblies. For these calculations we have used model DBA systems with two $OC_{16}H_{33}$ chains and the remaining four positions that do not participate directly in intermolecular interactions at the level of DBA dimers were truncated with small rigid alkoxy chains. Full molecular structures of the optimized models are given in (Supporting Information, section S10).

of the alkyl chains with the graphite lattice underneath, tilting the alkyl chains with respect to the DBA core (Figure 8b). Similar tilting is also observed in maximization of the van der Waals interactions between interdigitating alkyl chains, both in terms of the interchain distance as well as the relative position of the methylene groups in adjacent chains (Figure 8c). Both effects work together, yielding the observed changes in molecular conformations of the DBA assemblies adsorbed on the HOPG (Figure 8d). Furthermore, optimized interactions (intra-, inter-, and substrate−molecule) are effectively translated throughout the supramolecular network *via* commensurability, clearly visible in periodic modulations of the STM contrast, a Moiré pattern, of the DBA cores (Supporting Information, Figure S13).

C_3-symmetric adsorbed DBA molecules are chiral with each pair of the coaligned alkyl chains on the surface acting as an origin of chirality. Thus, in addition to supramolecular chirality (Figure 1) arising from the interdigitation of the alkyl chains on the surface, each DBA molecule possesses also specific molecular (point group) chirality, denoted as *R*-**DBA** or *S*-**DBA** (Figure 9a). An analysis of high resolution STM images confirms nonorthogonal tilt (*R*-**DBA** or *S*-**DBA**) of the alkyl chains with respect to the side of the DBA core (Figure 9c,d).

At the level of DBA dimers four different combinations are possible (Figure 9b), with *R*(+)/*S*(−) and *R*(−)/*S*(+)) being enantiomeric pairs. Intriguingly, existence of a specific combination depends on the parity of carbons in the alkoxy chains: *R*(+) and *S*(−) for **DBA-OCn$_{even}$**, while *R*(−) and *S*(+) are the most favorable for **DBA-OCn$_{odd}$** (Figure 9c,d).

To the best of our knowledge, this is the first example of the odd−even effect in porous 2D assemblies. It arises from the asymmetry in van der Waals interactions of the interdigitated alkyl chains and DBA core (Figure 10). Because alkyl chains are known to align along main symmetry axes of graphite,[47] the overall alignment of DBA assemblies with respect to the graphite is also structure-specific and our modeling is in very good agreement with the experimental data (Supporting Information, section S10 and Figure S16).

Our calculations also suggest that chiral domains with perfect hexagonal lattice are the thermodynamic minimum structures of monocomponent DBA assemblies. Less symmetric hexagons (Figure 1) are formed from diastereomeric pairs (*R*(+)/*R*(−) or *S*(+)/*S*(−)) and, as such, are less stable than homochiral assemblies formed from C_6-hexagons. The metastable nature of irregular hexagons in monocomponent DBA assemblies is also evident from thermal annealing

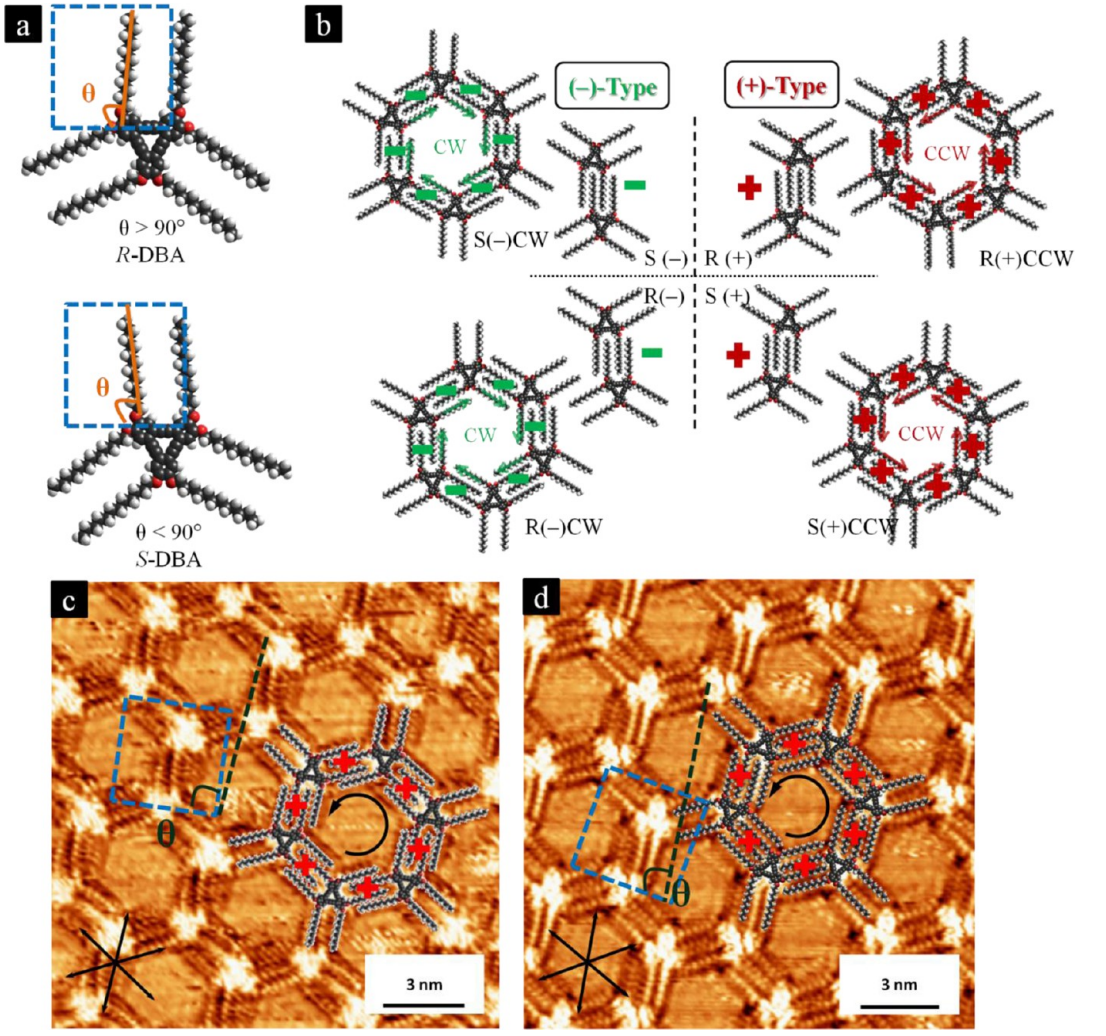

Figure 9. (a) Prochiral DBA compounds upon adlayer formation. Depending on whether the angle is $\theta > 90°$ or $\theta < 90°$, a *R*-DBA or *S*-DBA will be formed, respectively. (b) Combining point group chirality of DBA compounds with organizational chirality of the alkyl chain interdigitation results in four different types of dimers and C_6-symmetric hexagons. (c) High resolution image of a CCW domain of DBA-OC12 (I_{set} = 0.2 nA and V_{bias} = −0.2 V). (d) High resolution image of a CCW domain of DBA-OC13 (I_{set} = 0.8 nA and V_{bias} = −0.15 V). The dotted blue square represents a 90° angle with respect to the core of the DBA compound. The values for θ measured experimentally (85 ± 3° and 95 ± 3°) are close to those predicted by the calculations.

experiments: at higher temperatures when kinetic trapping is reduced only regular DBA hexagons remain on the surface (Figure S11). Stability of irregular hexagons can be improved by coadsorption of suitable guest. Indeed, we have recently reported a highly ordered three-component assembly that contains both C_3- and C_6-symmetric DBA hexagons.[48]

Modeling self-assembly of heterodimers composed of two different DBAs (**DBA-OCn$_{odd}$** + **DBA-OCn$_{even}$**) showed another manifestation of the odd−even effect. Depending on the parity of the longer alkoxy chains two structurally different thermodynamic minima are predicted (Figure 11).

If $n_{odd} > n_{even}$, the energy of intermolecular interactions of the heterodimer is lower than the average of intermolecular binding energies of the homodimers built from its components. Unlike monocomponent assemblies (Figure 8d), maximization of the overall stability of these heteroassemblies is achieved with some compromises: a mismatched interdigitation of the alkyl chains, and ineffective packing with a gap between some of the methyl groups of **DBA-OCn$_{even}$** and DBA cores of **DBA-OCn$_{odd}$** (Figure 11). These factors render mixing such DBAs thermodynamically unfavorable thus explaining phase separation observed experimentally (Figure 2a,b). The observed preferential adsorption of the smaller **DBA-OCn$_{even}$** over the adsorption of **DBA-OCn$_{odd}$** can be attributed to the synergy of both kinetic and thermodynamic factors. Namely, being smaller, **DBA-OCn$_{even}$** has a lower reorganization barrier than corresponding **DBA-OCn$_{odd}$**. Therefore, **DBA-OCn$_{even}$** domains are expected to grow faster. Furthermore, **DBA-OCn$_{even}$** domains have a higher surface density than **DBA-OCn$_{odd}$** domains, that is, a larger number of interactions per surface

area, and therefore, **DBA-OCn$_{even}$** are thermodynamically more stable.

The occasional inclusion of **DBA-OCn$_{even}$** into the network of larger **DBA-OCn$_{odd}$** happens (Figure 6b and the related part in Results) because it does not alter the structure of the latter (isomorphic substitution). Obviously, the opposite, that is, inclusion of the larger **DBA-OCn$_{odd}$** into the domains of pure **DBA-OCn$_{even}$**, causes significant lattice distortion because of steric constraints and is highly unfavorable. Similar to monocomponent DBA self-assembly, all non-C_6-symmetric hexagons observed in these mixtures are kinetically trapped formations which disappear at higher temperature (Supporting Information, section S8).

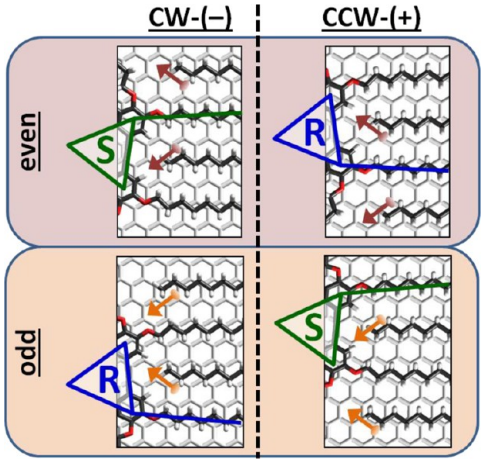

Figure 10. Asymmetric interactions responsible for the odd–even effect in DBA assemblies and relationship between the parity of the alkyl chains, molecular and supramolecular chiralities. Optimization of different interactions leads to the formation of only two thermodynamic minima for each DBA homoassembly: *R*(+) and *S*(−) for DBA-OCn$_{even}$ and *R*(−) and *S*(+) for DBA-OCn$_{odd}$. Dark-red and orange arrows show the directions of the methyl groups in homoassemblies of DBA-OCn$_{even}$ and DBA-OCn$_{odd}$, respectively. Blue and red triangles represent the orientation of the DBA cores and denote molecular chirality.

If $n_{odd} < n_{even}$, the energy of intermolecular interactions of the heterodimer is higher than the average of intermolecular binding energies of the homodimers built from its components (Figure 11), thus, leading to a favorable mixing of both DBAs. For these mixtures, unlike the case of the phase separating combinations discussed above, molecular modeling predicts matched interdigitation of the alkyl chains (Figure 11) as well as additional van der Waals interactions (Figure 12e).

Self-assembly formed at room temperature is a two-dimensional short-range disordered molecular crystalline network,[49−51] because in addition to bimodal interdigitation ("+" and "−") and two-component coassembly (**DBA-OCn$_{odd}$** and **DBA-OCn$_{even}$**), molecular chirality of each DBA also varies. Overcoming kinetic barriers at higher temperatures results in the formation of a new highly ordered polymorph composed of **DBA-OCn$_{even}$** C_6-hexamers connected *via* **DBA-OCn$_{odd}$** (Figure 12a) to maximize the intermolecular interaction (Figure 12e). It is different from the recently reported DBA self-assembly stabilized *via* host−guest interactions[52] and represents a unique level of complexity in that not only composition and spatial order, but also molecular and supramolecular chirality, of the components are well-defined. Formed even in the excess of **DBA-OCn$_{odd}$** this structure represents the thermodynamically stable polymorph composed of both DBAs.

CONCLUSIONS

In conclusion, we have investigated the unusual phase behavior of alkylated molecules that self-assemble into a nanoporous phase. The system shows

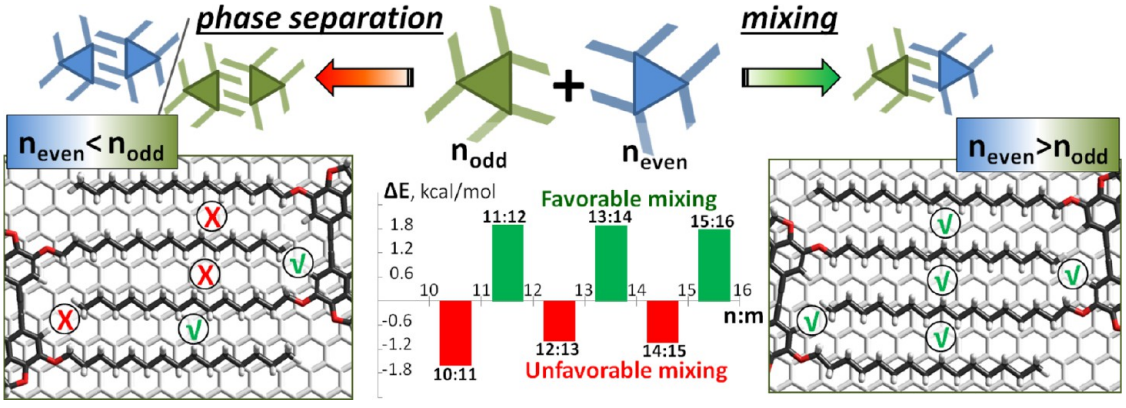

Figure 11. Behavior of bicomponent DBA mixtures (DBA-OCn$_{odd}$ + DBA-OCn$_{even}$) leading to the phase separation (left) or mixing (right) due to unfavorable or favorable stabilization energy (ΔE) of the heterodimers, respectively. $\Delta E = E_{odd-even} - 0.5(E_{odd-odd} + E_{even-even})$, where $E_{odd-even}$ is the interaction energy of the heterodimer (DBA-OCn$_{odd}$ + DBA-OCn$_{even}$), while $E_{odd-odd}$ and $E_{even-even}$ are respective energies of the homodimers (DBA-OCn$_{odd}$ + DBA-OCn$_{odd}$ and DBA-OCn$_{even}$ + DBA-OCn$_{even}$). Differences in the interaction energies of the mixtures are the result of matched/mismatched interdigitation of alkyl chains and presence/absence of tight packing featuring additional van der Waals interactions between terminal methyl groups and DBA cores. Schematically, interactions responsible for favorable/unfavorable mixing of DBAs are marked with green ticks/red crosses, respectively.

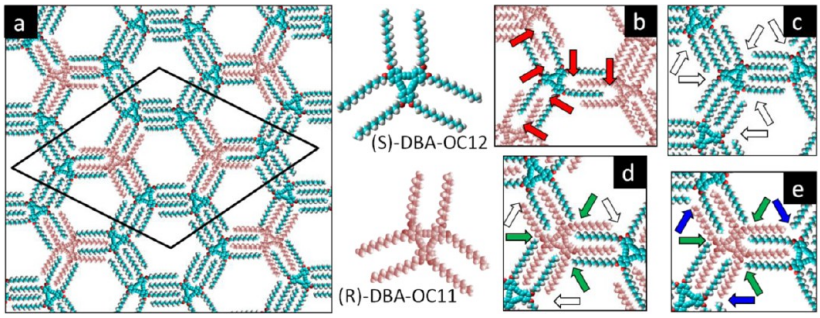

Figure 12. (a) Supramolecular structure of the highly ordered 2D coassembly formed from DBA-OC11 and DBA-OC12 after thermal annealing at liquid−solid interface. All DBA molecules have well-defined spatial position, chemical nature (DBA-OC11 or DBA-OC12), and molecular (*R*- or *S*-enantiomer) and supramolecular ("−" or "+") chirality. This model is in good agreement with the experimental data. Alternative arrangements (the figures b and d) contradict STM observations and are expected to be less stable. Thus, the structure shown in (b) has the wrong molecular chirality and inefficient packing (marked with red arrows), while the structure shown in (d) has the wrong supramolecular chirality and is missing some of the additional van der Waals contacts (marked with blue arrows) found in the proposed structure of the coassembly (e). For convenience, additional van der Waals contacts between the end of the alkyl chain and the side of the alkyl chain or the ends of the alkyl chains absent in monocomponent DBA assemblies (c) are marked with green and blue arrows in the figures (d) and (e).

a high level of complexity exhibiting all possible mixing phenomena: phase separation, preferential adsorption, perfect mixing, and cocrystallization. Also, in the course of this study we have found the first example of an odd−even effect in 2D porous networks and revealed the origins of molecular chirality in DBA assemblies. The methodology and analysis presented in this work can be easily adapted for the investigation of self-assembly of other alkylated building blocks. Also, understanding the mechanisms leading to different phase behavior opens interesting practical possibilities. For example, we are currently exploring chiral induction in mixtures of structurally different components. Under conditions of favorable heterointeractions, this will allow to broaden the scope of highly effective chiral inductors to new systems.

MATERIALS AND METHODS

The stock solutions of the achiral DBA derivatives were prepared in 1-phenyloctane (Sigma-Aldrich; 5.0×10^{-4} M). These pure solutions were then diluted. The mixed solutions were prepared by mixing together the two compounds at high concentration ($\sim 10^{-4}$ M) in a 1:1 molar ratio and subsequently diluting the sample overall concentration. All samples were subsequently drop-casted (12 μL) onto the basal (0001) plane of freshly cleaved highly oriented pyrolytic graphite (HOPG, grade ZYB, Advanced Ceramics Inc., Cleveland, OH, U.S.A.). Within 2 h, visualization of the spontaneously formed surface-supported molecular networks was realized using scanning tunneling microscopy (STM - PicoSPM (Agilent)) in constant current mode at the liquid/solid interface. All STM images were acquired at room temperature (20−23 °C), unless stated otherwise. The tips were mechanically cut from Pt/Ir (80/20, ∅ 0.25 mm) wire. Several samples were investigated, and for each sample, several locations were probed. Analysis was performed after drift correction by using SPIP software (Image Metrology A/S) or WSxM.[53]

All molecular mechanics calculations were performed with MM+ force field, as implemented in HyperChem Prof. 7.52.[4] Geometries were optimized to rms deviation of the energy gradient smaller than 0.01 kcal/(mol·Å). Supporting DFT calculations were carried out with Gaussian G09[5] applying symmetry constrains (if appropriate) to reduce computational costs. Further details about computational methods can be found in the Supporting Information, section S10.

Conflict of Interest: The authors declare no competing financial interest.

Supporting Information Available: Synthesis procedures, additional STM images, STM experimental procedures and analysis details, and molecular modeling simulation details. This material is available free of charge *via* the Internet at http://pubs.acs.org.

Acknowledgment. This work is supported by the Fund of Scientific Research − Flanders (FWO), the Agency for Innovation by Science and Technology in Flanders (IWT), KU Leuven (GOA), the Belgian Federal Science Policy Office through IAP-7/05, the Hercules foundation, Grant-in-Aid for Scientific Research from the Ministry of Education, Culture, Sports, Science, and Technology, Japan (21245012, 23111710).

REFERENCES AND NOTES

1. Kim, D. H.; Park, Y. D.; Jang, Y. S.; Yang, H. C.; Kim, Y. H.; Han, J. I.; Moon, D. G.; Park, S. J.; Chang, T. Y.; Chang, C. W.; et al. Enhancement of Field-Effect Mobility Due to Surface-Mediated Molecular Ordering in Regioregular Polythiophene Thin Film Transistors. *Adv. Funct. Mater.* **2005**, *15*, 77–82.
2. Madueno, R.; Raisanen, M. T.; Silien, C.; Buck, M. Functionalizing Hydrogen-Bonded Surface Networks with Self-Assembled Monolayers. *Nature* **2008**, *454*, 618–621.
3. Balaur, E.; Macak, J. M.; Taveira, L.; Schmuki, P. Tailoring the Wettability of TiO_2 Nanotube Layers. *Electrochem. Commun.* **2005**, *7*, 1066–1070.
4. Khodabakhsh, S.; Sanderson, B. M.; Nelson, J.; Jones, T. S. Using Self-Assembling Dipole Molecules to Improve Charge Collection in Molecular Solar Cells. *Adv. Funct. Mater.* **2006**, *16*, 95–100.
5. Wan, X.; Chen, K.; Du, J.; Liu, D. Q.; Chen, J.; Lai, X.; Xie, W. G.; Xu, J. B. Enhanced Performance and Fermi-Level Estimation of Coronene-Derived Graphene Transistors on Self-Assembled Monolayer Modified Substrates in Large Areas. *J. Phys. Chem. C* **2013**, *117*, 4800–4807.
6. Halik, M.; Hirsch, A. The Potential of Molecular Self-Assembled Monolayers in Organic Electronic Devices. *Adv. Mater.* **2011**, *23*, 2689–2695.
7. Bejarano-Villafuerte, A.; van der Meijden, M. W.; Lingenfelder, M.; Wurst, K.; Kellogg, R. M.; Amabilino, D. B. A Chiral

Self-Assembled Monolayer Derived from a Resolving Agent and Its Performance as a Crystallization Template for an Organic Compound from Organic Solvents. *Chem.—Eur. J.* **2012**, *18*, 15984–15993.
8. De Cat, I.; Gobbo, C.; Van Averbeke, B.; Lazzaroni, R.; De Feyter, S.; van Esch, J. Controlling the Position of Functional Groups at the Liquid/Solid Interface: Impact of Molecular Symmetry and Chirality. *J. Am. Chem. Soc.* **2011**, *133*, 20942–20950.
9. Ahn, S.; Matzger, A. J. Six Different Assemblies from One Building Block: Two-Dimensional Crystallization of an Amide Amphiphile. *J. Am. Chem. Soc.* **2010**, *132*, 11364–11371.
10. den Boer, D.; Habets, T.; Coenen, M. J. J.; van der Maas, M.; Peters, T. P. J.; Crossley, M. J.; Khoury, T.; Rowan, A. E.; Nolte, R. J. M.; Speller, S.; et al. Controlled Templating of Porphyrins by a Molecular Command Layer. *Langmuir* **2011**, *27*, 2644–2651.
11. Takajo, D.; Inaba, A.; Isoda, S. Preferential Adsorption Followed by Spontaneous Desorption of 1-Octadecanol at a Solution/Graphite Interface. *Thin Solid Films* **2010**, *519*, 1371–1374.
12. Raval, R. Nanoscale Insights into the Creation of Chiral Surfaces. *J. Mol. Catal. A: Chem.* **2009**, *305*, 112–116.
13. Theobald, J. A.; Oxtoby, N. S.; Phillips, M. A.; Champness, N. R.; Beton, P. H. Controlling Molecular Deposition and Layer Structure with Supramolecular Surface Assemblies. *Nature* **2003**, *424*, 1029–1031.
14. Jurak, M. Thermodynamic Aspects of Cholesterol Effect on Properties of Phospholipid Monolayers: Langmuir and Langmuir-Blodgett Monolayer Study. *J. Phys. Chem. B* **2013**, *117*, 3496–3502.
15. Palma, C.-A.; Bjork, J.; Bonini, M.; Dyer, M. S.; Llanes-Pallas, A.; Bonifazi, D.; Persson, M.; Samori, P. Tailoring Bicomponent Supramolecular Nanoporous Networks: Phase Segregation, Polymorphism, and Glasses at the Solid–Liquid Interface. *J. Am. Chem. Soc.* **2009**, *131*, 13062–13071.
16. Pint, C. L.; Roth, M. W. Simulated Effects of Odd-Alkane Impurities in a Hexane Monolayer on Graphite. *Phys. Rev. B* **2006**, *73*, 115404.
17. Bickerstaffe, A.; Messe, L.; Clarke, S. M.; Parker, J.; Perdigon, A.; Cheah, N. P.; Inaba, A. Mixing Behaviour of Carboxylic Acids Adsorbed on Graphite. *Phys. Chem. Chem. Phys.* **2004**, *6*, 3545–3550.
18. Wang, R.; Mao, H. Y.; Huang, H.; Qi, D. C.; Chen, W. Scanning Tunneling Microscopy and Photoelectron Spectroscopy Investigation of the Sexithiophene: C-60 Donor-Acceptor Nanostructure Formation on Graphite. *J. Appl. Phys.* **2011**, *109*, 084307.
19. Messe, L.; Clarke, S. M.; Arnold, T.; Dong, C.; Thomas, R. K.; Inaba, A. Mixing Behavior at the Solid/Liquid Interface: Binary Monolayers of Linear Alcohols Adsorbed on Graphite. *Langmuir* **2002**, *18*, 4010–4013.
20. Stohr, M.; Boz, S.; Schar, M.; Nguyen, M. T.; Pignedoli, C. A.; Passerone, D.; Schweizer, W. B.; Thilgen, C.; Jung, T. A.; Diederich, F. Self-Assembly and Two-Dimensional Spontaneous Resolution of Cyano-Functionalized 7 Helicenes on Cu(111). *Angew. Chem., Int. Ed.* **2011**, *50*, 9982–9986.
21. Xue, Y.; Zimmt, M. B. Patterned Monolayer Self-Assembly Programmed by Side Chain Shape: Four-Component Gratings. *J. Am. Chem. Soc.* **2012**, *134*, 4513–4516.
22. Silly, F.; Shaw, A. Q.; Castell, M. R.; Briggs, G. A. D. A Chiral Pinwheel Supramolecular Network Driven by the Assembly of Ptcdi and Melamine. *Chem. Commun.* **2008**, 1907–1909.
23. Clarke, S. M.; Messe, L.; Adams, J.; Inaba, A.; Arnold, T.; Thomas, R. K. A Quantitative Parameter for Predicting Mixing Behaviour in Adsorbed Layers: The 2D Isomorphism Coefficient. *Chem. Phys. Lett.* **2003**, *373*, 480–485.
24. Wintgens, D.; Yablon, D. G.; Flynn, G. W. Packing of $HO(CH_2)_{14}COOH$ and $HO(CH_2)_{15}COOH$ on Graphite at the Liquid–Solid Interface Observed by Scanning Tunneling Microscopy: Methylene Unit Direction of Self-Assembly Structures. *J. Phys. Chem. B* **2003**, *107*, 173–179.
25. Katsouras, I.; Geskin, V.; Kronemeijer, A. J.; Blom, P. W. M.; de Leeuw, D. M. Binary Self-Assembled Monolayers: Apparent Exponential Dependence of Resistance on Average Molecular Length. *Org. Electron.* **2011**, *12*, 857–864.
26. Messe, L.; Clarke, S. M.; Dong, C. C.; Thomas, R. K.; Inaba, A.; Alba, M. D.; Castro, M. A. Mixing Behavior at the Solid/Liquid Interface: Binary Alcohol Monolayers on Graphite. *Langmuir* **2002**, *18*, 9429–9433.
27. Wang, G. J.; Lei, S. B.; De Feyter, S.; Feldman, R.; Parker, J. E.; Clarke, S. M. Behavior of Binary Alcohol Mixtures Adsorbed on Graphite Using Calorimetry and Scanning Tunneling Microscopy. *Langmuir* **2008**, *24*, 2501–2508.
28. Castro, M. A.; Clarke, S. M.; Inaba, A.; Arnold, T.; Thomas, R. K. The Investigation of Mixed Monolayers Adsorbed from Solution: Octane and Nonane Mixtures on Graphite. *Phys. Chem. Chem. Phys.* **1999**, *1*, 5017–5023.
29. Castro, M.; Clarke, S. M.; Inaba, A.; Thomas, R. K.; Arnold, T. Adsorption Behaviour of the Binary Mixtures of Octane and Nonane at Sub-Monolayer Coverage on Graphite. *Phys. Chem. Chem. Phys.* **2001**, *3*, 3774–3777.
30. Ramin, L.; Jabbarzadeh, A. Odd–Even Effects on the Structure, Stability, and Phase Transition of Alkanethiol Self-Assembled Monolayers. *Langmuir* **2011**, *27*, 9748–9759.
31. Liu, X. F.; Wang, T. Y.; Liu, M. H. Interfacial Assembly of a Series of Cinnamoyl-Containing Bolaamphiphiles: Spacer-Controlled Packing, Photochemistry, and Odd–Even Effect. *Langmuir* **2012**, *28*, 3474–3482.
32. Nerngchamnong, N.; Yuan, L.; Qi, D. C.; Li, J.; Thompson, D.; Nijhuis, C. A. The Role of van der Waals Forces in the Performance of Molecular Diodes. *Nat. Nanotechnol.* **2013**, *8*, 113–118.
33. Tao, F.; Bernasek, S. L. Understanding Odd–Even Effects in Organic Self-Assembled Monolayers. *Chem. Rev.* **2007**, *107*, 1408–1453.
34. Xu, L.; Miao, X. R.; Zha, B.; Deng, W. L. Hydrogen-Bonding-Induced Polymorphous Phase Transitions in 2D Organic Nanostructures. *Chem. Asian J.* **2013**, *8*, 926–933.
35. Yablon, D. G.; Guo, J. S.; Knapp, D.; Fang, H. B.; Flynn, G. W. Scanning Tunneling Microscopy Investigation of a Chirally Pure Molecule at the Liquid-Solid Interface: Unambiguous Topographic Markers. *J. Phys. Chem. B* **2001**, *105*, 4313–4316.
36. Tao, F.; Goswami, J.; Bernasek, S. L. Self-Assembly and Odd–Even Effects of *cis*-Unsaturated Carboxylic Acids on Highly Oriented Pyrolytic Graphite. *J. Phys. Chem. B* **2006**, *110*, 4199–4206.
37. Henze, O.; Feast, W. J.; Gardebien, F.; Jonkheijm, P.; Lazzaroni, R.; Leclere, P.; Meijer, E. W.; Schenning, A. Chiral Amphiphilic Self-Assembled α,α'-Linked Quinque-, Sexi-, and Septithiophenes: Synthesis, Stability, and Odd–Even Effects. *J. Am. Chem. Soc.* **2006**, *128*, 5923–5929.
38. Wei, Y. H.; Kannappan, K.; Flynn, G. W.; Zimmt, M. B. Scanning Tunneling Microscopy of Prochiral Anthracene Derivatives on Graphite: Chain Length Effects on Monolayer Morphology. *J. Am. Chem. Soc.* **2004**, *126*, 5318–5322.
39. Li, M.; Zeng, Q.; Wang, C. Self-Assembled Supramolecular Networks at Interfaces: Molecular Immobilization and Recognition Using Nanoporous Templates. *Sci. China: Phys., Mech. Astron.* **2011**, *54*, 1739–1748.
40. Pawin, G.; Wong, K. L.; Kwon, K. Y.; Bartels, L. A Homomolecular Porous Network at a Cu(111). *Surf. Sci.* **2006**, *313*, 961–962.
41. Popoff, A.; Fichou, D. Weak Intermolecular H-Bonds as a Tool to Design 2D Self-Organized Molecular Architectures: Tailoring a "Scottish Tartan" Open Network. *J. Mol. Struct.* **2009**, *936*, 156–161.
42. Kuhne, D.; Klappenberger, F.; Decker, R.; Schlickum, U.; Brune, H.; Klyatskaya, S.; Ruben, M.; Barth, J. V. Self-Assembly of Nanoporous Chiral Networks with Varying Symmetry from Sexiphenyl-Dicarbonitrile on Ag(111). *J. Phys. Chem. C* **2009**, *113*, 17851–17859.
43. Lei, S. B.; Tahara, K.; Adisoejoso, J.; Balandina, T.; Tobe, Y.; De Feyter, S. Towards Two-Dimensional Nanoporous

Networks: Crystal Engineering at the Solid-Liquid Interface. *CrystEngComm* **2010**, *12*, 3369–3381.
44. Lei, S.; Tahara, K.; Müllen, K.; Szabelski, P.; Tobe, Y.; De Feyter, S. Mixing Behavior of Alkoxylated Dehydrobenzo-[12]Annulenes at the Solid−Liquid Interface: Scanning Tunneling Microscopy and Monte Carlo Simulations. *ACS Nano* **2011**, *5*, 4145–4157.
45. Tahara, K.; Furukawa, S.; Uji-I, H.; Uchino, T.; Ichikawa, T.; Zhang, J.; Mamdouh, W.; Sonoda, M.; De Schryver, F. C.; De Feyter, S.; et al. Two-Dimensional Porous Molecular Networks of Dehydrobenzo[12]Annulene Derivatives *via* Alkyl Chain Interdigitation. *J. Am. Chem. Soc.* **2006**, *128*, 16613–16625.
46. Tahara, K.; Yamaga, H.; Ghijsens, E.; Inukai, K.; Adisoejoso, J.; Blunt, M. O.; De Feyter, S.; Tobe, Y. Control and Induction of Surface-Confined Homochiral Porous Molecular Networks. *Nat. Chem.* **2011**, *3*, 714–719.
47. Cyr, D. M.; Venkataraman, B.; Flynn, G. W. STM Investigations of Organic Molecules Physisorbed at the Liquid−Solid Interface. *Chem. Mater.* **1996**, *8*, 1600–1615.
48. Balandina, T.; Tahara, K.; Sändig, N.; Blunt, M. O.; Adisoejoso, J.; Lei, S.; Zerbetto, F.; Tobe, Y.; De Feyter, S. Role of Substrate in Directing the Self-Assembly of Multicomponent Supramolecular Networks at the Liquid−Solid Interface. *ACS Nano* **2012**, *6*, 8381–8389.
49. Blunt, M. O.; Russell, J. C.; Giménez-López, M. d. C.; Garrahan, J. P.; Lin, X.; Schröder, M.; Champness, N. R.; Beton, P. H. Random Tiling and Topological Defects in a Two-Dimensional Molecular Network. *Science* **2008**, *322*, 1077–1081.
50. Zhou, H.; Dang, H.; Yi, J.-H.; Nanci, A.; Rochefort, A.; Wuest, J. D. Frustrated 2D Molecular Crystallization. *J. Am. Chem. Soc.* **2007**, *129*, 13774–13775.
51. Ecija, D.; Vijayaraghavan, S.; Auwärter, W.; Joshi, S.; Seufert, K.; Aurisicchio, C.; Bonifazi, D.; Barth, J. V. Two-Dimensional Short-Range Disordered Crystalline Networks from Flexible Molecular Modules. *ACS Nano* **2012**, *6*, 4258–4265.
52. Destoop, I.; Ghijsens, E.; Katayama, K.; Tahara, K.; Mali, K. S.; Tobe, Y.; De Feyter, S. Solvent-Induced Homochirality in Surface-Confined Low-Density Nanoporous Molecular Networks. *J. Am. Chem. Soc.* **2012**, *134*, 19568–19571.
53. Horcas, I.; Fernandez, R.; Gomez-Rodriguez, J. M.; Colchero, J.; Gomez-Herrero, J.; Baro, A. M. WSXM: A Software for Scanning Probe Microscopy and a Tool for Nanotechnology. *Rev. Sci. Instrum.* **2007**, *78*, 013705.